Thyroid hormone receptors mediate two distinct mechanisms of long-wavelength vision

Leo I. Volkov[a], Jeong Sook Kim-Han[b], Lauren M. Saunders[c,d], Deepak Poria[e], Andrew E. O. Hughes[a], Vladimir J. Kefalov[e], David M. Parichy[c,d], and Joseph C. Corbo[a,1]

[a]Department of Pathology and Immunology, Washington University School of Medicine, St. Louis, MO 63110; [b]Department of Pharmacology, A.T. Still University of Health Sciences, Kirksville, MO 63501; [c]Department of Biology, University of Virginia, Charlottesville, VA 22903; [d]Department of Cell Biology, University of Virginia, Charlottesville, VA 22903; and [e]Department of Ophthalmology and Visual Sciences, Washington University School of Medicine, St. Louis, MO 63110

Edited by Jeremy Nathans, Johns Hopkins University School of Medicine, Baltimore, MD, and approved May 14, 2020 (received for review November 14, 2019)

Thyroid hormone (TH) signaling plays an important role in the regulation of long-wavelength vision in vertebrates. In the retina, *thyroid hormone receptor β* (*thrb*) is required for expression of long-wavelength-sensitive opsin (*lws*) in red cone photoreceptors, while in retinal pigment epithelium (RPE), TH regulates expression of a cytochrome P450 enzyme, *cyp27c1*, that converts vitamin A_1 into vitamin A_2 to produce a red-shifted chromophore. To better understand how TH controls these processes, we analyzed the phenotype of zebrafish with mutations in the three known TH nuclear receptor transcription factors (*thraa*, *thrab*, *and thrb*). We found that no single TH nuclear receptor is required for TH-mediated induction of *cyp27c1* but that deletion of all three (*thraa*$^{-/-}$;*thrab*$^{-/-}$;*thrb*$^{-/-}$) completely abrogates its induction and the resulting conversion of A_1- to A_2-based retinoids. In the retina, loss of *thrb* resulted in an absence of red cones at both larval and adult stages without disruption of the underlying cone mosaic. RNA-sequencing analysis revealed significant down-regulation of only five genes in adult *thrb*$^{-/-}$ retina, of which three (*lws1*, *lws2*, and *miR-726*) occur in a single syntenic cluster. In the *thrb*$^{-/-}$ retina, retinal progenitors destined to become red cones were transfated into ultraviolet (UV) cones and horizontal cells. Taken together, our findings demonstrate cooperative regulation of *cyp27c1* by TH receptors and a requirement for *thrb* in red cone fate determination. Thus, TH signaling coordinately regulates both spectral sensitivity and sensory plasticity.

thyroid hormone | retinal development | cone photoreceptors | vitamin A_2 | zebrafish

The spectral sensitivity of a visual pigment is determined by the amino acid sequence of the opsin protein and the chemical structure of its covalently bound, vitamin A-based chromophore (1, 2). In the course of evolution, opsin gene duplication followed by the divergence of amino acid sequences involved in spectral tuning has resulted in a multiplicity of opsins with peak spectral sensitivities ranging from UV to red (3). For example, zebrafish possess four cone photoreceptor subtypes that each express a different opsin: UV cone opsin (*sws1*), blue cone opsin (*sws2*), green cone opsin (*rh2*), and red cone opsin (*lws*) (Fig. 1*A*). The zebrafish genome contains two red cone opsin paralogs (*lws1* and *lws2*) and four green cone opsin paralogs (*rh2-1*, *rh2-2*, *rh2-3*, and *rh2-4*) (4, 5).

The spectral sensitivities of photoreceptors appear to be stable across the lifespan of most avian and mammalian species (3). In contrast, numerous species of aquatic vertebrates are capable of dynamically tuning their spectral sensitivities at different stages of the life cycle or in response to changing environmental conditions (6, 7). For example, when salmon or lamprey migrate from the blue-green waters of the open ocean to the red-shifted spectral milieu of inland streams to spawn, they shift the spectral sensitivity of their visual system to match that of the new environment (8–10). This shift is primarily mediated by the expression of a cytochrome P450 enzyme, *cyp27c1*, which converts vitamin A_1 into vitamin A_2 to produce a red-shifted chromophore in the retinal pigment epithelium (RPE) (Fig. 1*A*) (9, 11). Replacement of the A_1-based chromophore, 11-*cis* retinaldehyde, with the A_2-based chromophore, 11-*cis* 3,4-didehydroretinaldehyde red-shifts the sensitivity of red cone opsins by nearly 60 nm (11, 12). Conversely, the A_1-to-A_2 shift has only a minimal effect on the spectral sensitivity of short wavelength-tuned opsins (i.e., UV- and blue-sensitive opsins) (11, 12). Therefore, the primary effect of *cyp27c1* expression is to extend the sensitivity of the longest wavelength-sensitive opsin further into the near infrared, thereby facilitating vision in turbid waters where longer wavelength light predominates. Despite the importance of this mechanism of sensory plasticity in aquatic vertebrates, the transcription factors that control *cyp27c1* expression are currently unknown. One clue to the mechanism of *cyp27c1* regulation is that exogenous application of TH induces an A_1-to-A_2 shift in the eyes of various teleost species (7, 12). This finding suggests a role for TH signaling in regulating *cyp27c1* expression.

TH signaling has also been shown to regulate opsin expression in the retina. The application of TH drives both the transition from UV cone opsin (*sws1*) to blue cone opsin (*sws2*) expression and the induction of a longer-wavelength-sensitive (red-shifted) green cone opsin (*rh2*) paralog in salmonid species (13, 14).

Significance

Spectral sensitivity is determined by the components of the light-sensitive visual pigment: an opsin protein and a covalently bound chromophore. Thyroid hormone signaling has been shown to regulate both the expression of long-wavelength (red) opsin and *cyp27c1*, an enzyme that converts the vitamin A_1-based chromophore to the red-shifted vitamin A_2-based form. Here, we show that all three zebrafish thyroid hormone nuclear receptors play a role in mediating induction of *cyp27c1* expression in response to thyroid hormone and that mutations in *thyroid hormone receptor β* result in an absence of red cones and the transfating of red cone precursors into UV cones and horizontal cells in zebrafish. These results demonstrate that thyroid hormone receptors regulate two distinct aspects of long-wavelength vision.

Author contributions: L.I.V., J.S.K.-H., D.P., V.J.K., and J.C.C. designed research; L.I.V., J.S.K.-H., and D.P. performed research; L.M.S. and D.M.P. contributed new reagents/analytic tools; L.I.V., J.S.K.-H., D.P., A.E.O.H., V.J.K., and J.C.C. analyzed data; and L.I.V. and J.C.C. wrote the paper.

The authors declare no competing interest.

This article is a PNAS Direct Submission.

Data deposition: RNA-seq data are available under Gene Expression Omnibus (GEO) (accession no. GSE143312).

[1]To whom correspondence may be addressed. Email: jcorbo@wustl.edu.

This article contains supporting information online at https://www.pnas.org/lookup/suppl/doi:10.1073/pnas.1920086117/-/DCSupplemental.

First published June 15, 2020.

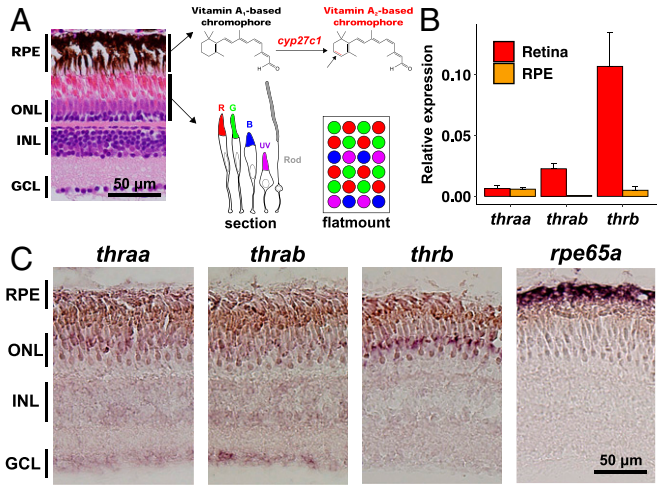

Fig. 1. TH receptor expression in zebrafish retina and RPE. (*A*) Hematoxylin and eosin-stained section of 9-mo-old zebrafish eye. The accompanying diagram shows *cyp27c1*-mediated conversion of 11-*cis* retinaldehyde (the vitamin A_1-based chromophore) into 11-*cis* 3,4-didehydroretinaldehyde (the vitamin A_2-based chromophore) in the RPE, and photoreceptor subtypes in the ONL. (*B*) Quantification of TH receptor expression in the retina and RPE of 5-mo-old WT zebrafish by qPCR. Relative expression (normalized to *rpl13a* expression [2^{-dCt}]; mean ± SD; $n = 3$ for all transcripts, except $n = 1$ for *thrab* in RPE due to lack of detectable transcript in two samples). (*C*) ISH of TH receptors in 9-mo-old *albino* zebrafish eye demonstrates that all TH receptors are expressed in the retina, whereas there is no detectable signal in the RPE. ISH with a probe against *rpe65a*, an RPE-specific gene, confirms the presence of RPE in the histologic sections.

Recent studies have shown that TH drives the expression of red-shifted green and red cone opsin paralogs in zebrafish as well (15). There is also evidence that *thrb* regulates the expression of red cone opsins and represses the expression of UV cone opsin orthologs in zebrafish, mouse, and human retinal organoids (16–18). Thus, TH signaling is likely to play an evolutionarily conserved role in the regulation of red cone opsin expression in vertebrates, thereby facilitating long-wavelength vision.

To elucidate the mechanisms by which TH receptors regulate long-wavelength vision, we analyzed the phenotype of zebrafish with mutations in the three known TH nuclear receptors: *thraa*, *thrab*, and *thrb*. We found that all three zebrafish TH receptors play a role in driving *cyp27c1* expression in RPE and that mutations in *thrb* result in an absence of red cones and transfating of red cone precursors into UV cones and horizontal cells in larvae. These results show how TH signaling mediates both spectral sensitivity and sensory plasticity.

Results

***thraa*, *thrab*, and *thrb* Redundantly Regulate *cyp27c1* Expression and the Vitamin A_1-to-A_2 Switch.** The zebrafish genome encodes three TH receptors: *thraa*, *thrab*, and *thrb* (19). To begin to evaluate the role of these receptors in zebrafish retina and RPE, we measured their expression by quantitative RT-PCR (qPCR). We found that all three receptors are expressed in the adult retina (Fig. 1*B* and *SI Appendix*, Fig. S1*A*). In RPE, in contrast, *thraa* and *thrb* are expressed while *thrab* is barely detectable (Fig. 1*B* and *SI Appendix*, Fig. S1*A*).

Next, we determined the cellular expression pattern of TH receptors by performing in situ hybridization (ISH) on adult *albino* zebrafish eyes (20). We used the *albino* strain to permit visualization of gene expression in RPE, which is heavily pigmented with melanin in wild-type (WT) fish. In the retina, we found *thraa* and *thrab* to be weakly expressed in all three layers (ONL, outer nuclear layer; INL, inner nuclear layer; and GCL, ganglion cell layer), whereas *thrb* expression was restricted to the ONL (Fig. 1*C*). The expression of all three receptors in the ONL appears to be restricted to a subset (or subsets) of photoreceptors, but the weakness of the *thraa* and *thrab* signals makes definitive assessment difficult. Publicly available single cell RNA-sequencing (RNA-seq) data from adult zebrafish retina confirm that *thraa* and *thrab* are broadly expressed across multiple retinal cell types, whereas *thrb* is specifically expressed in cones (21). In RPE, we were unable to detect any signal above background for any of the TH receptors by ISH (Fig. 1*C*). A strong signal for *rpe65a*, an RPE-specific transcript, confirmed the presence of RPE in our histologic sections (Fig. 1*C*).

To determine which TH receptors mediate TH-driven induction of *cyp27c1* expression and the resultant vitamin A_1-to-A_2 switch, we measured these processes in TH receptor mutant zebrafish. For this purpose, we utilized previously published zebrafish lines with mutations in *thraa* and *thrab* (22). In addition, we used CRISPR-Cas9 technology to engineer two *thrb* mutant alleles: $thrb^{stl627}$ (which contains a 25-bp deletion in exon 9) and $thrb^{stl628}$ (which contains a 52-bp deletion in exon 9). Both *thrb* mutant lines are predicted to result in a frame shift followed by a premature stop codon. These lines will both herein be referred to as $thrb^{-/-}$. All TH receptor mutations used in this study are predicted to truncate the receptor upstream of the ligand-binding domain (*Materials and Methods* and *SI Appendix*, Fig. S2). To evaluate the role of individual TH receptors in the TH-mediated induction of *cyp27c1* expression, we maintained $thraa^{-/-}$, $thrab^{-/-}$, and $thrb^{-/-}$ zebrafish and WT control fish in water containing TH (300 μg/L L-thyroxine) or vehicle for 3 wk. We then used qPCR to quantify *cyp27c1* expression and high-performance liquid chromatography (HPLC) to measure the relative amounts of A_1 and A_2 retinaldehydes. TH treatment resulted in robust induction of *cyp27c1* expression and a marked increase in A_2 retinaldehyde content in all three mutants and WT controls (Fig. 2 *A*–*F*). Although no reduction in *cyp27c1* expression was observed in TH-treated mutants, there was a statistically significant decrease in A_2 content in TH-treated $thraa^{-/-}$ fish relative to vehicle-treated mutants (Fig. 2 *A* and *D*). $thrab^{-/-}$ and $thrb^{-/-}$ fish displayed normal *cyp27c1* induction and A_2 content (Fig. 2 *B*, *C*, *E*, and *F*). Thus, no single TH receptor is required for induction of *cyp27c1* expression and A_1-to-A_2 conversion.

To assess whether the various TH receptors might act redundantly, we intercrossed the three mutant lines to create all possible double and triple mutant combinations. We then exposed the fish to either TH or vehicle and measured *cyp27c1* expression and A_1 and A_2 content. All double mutant fish showed reduced A_2 content (Fig. 2 *K*–*M*), whereas only $thraa^{-/-};thrb^{-/-}$ fish displayed a statistically significant decrease in *cyp27c1* induction (Fig. 2 *G*–*I*). Despite the relatively severe reduction in A_2 content in $thraa^{-/-};thrb^{-/-}$ fish, there appeared to be some residual induction of *cyp27c1* expression in this mutant relative to vehicle controls (Fig. 2*I*). Only in $thraa^{-/-};thrab^{-/-};thrb^{-/-}$ fish that lack all functional TH receptors, was there a complete failure of *cyp27c1* induction and A_2 production in response to TH treatment (Fig. 2 *J* and *N*). Thus, all three TH receptors appear to contribute to TH-mediated induction of *cyp27c1* expression and A_2 retinoid production, with *thraa* and *thrb* appearing to be most important.

Red Cones Are Absent from $thrb^{-/-}$ Retinas. A prior study demonstrated loss of red cone opsin expression in larval zebrafish using morpholinos targeting *thrb* (16). However, morpholino-induced phenotypes sometimes differ from those of the corresponding mutants, and the action of morpholinos is limited to the early larval stage (23). It also remains unclear whether the *thrb* morpholino phenotype is due to a simple loss of opsin expression or a defect in red cone fate determination. To address these questions, we analyzed the retinal phenotype of $thrb^{-/-}$ fish at larval

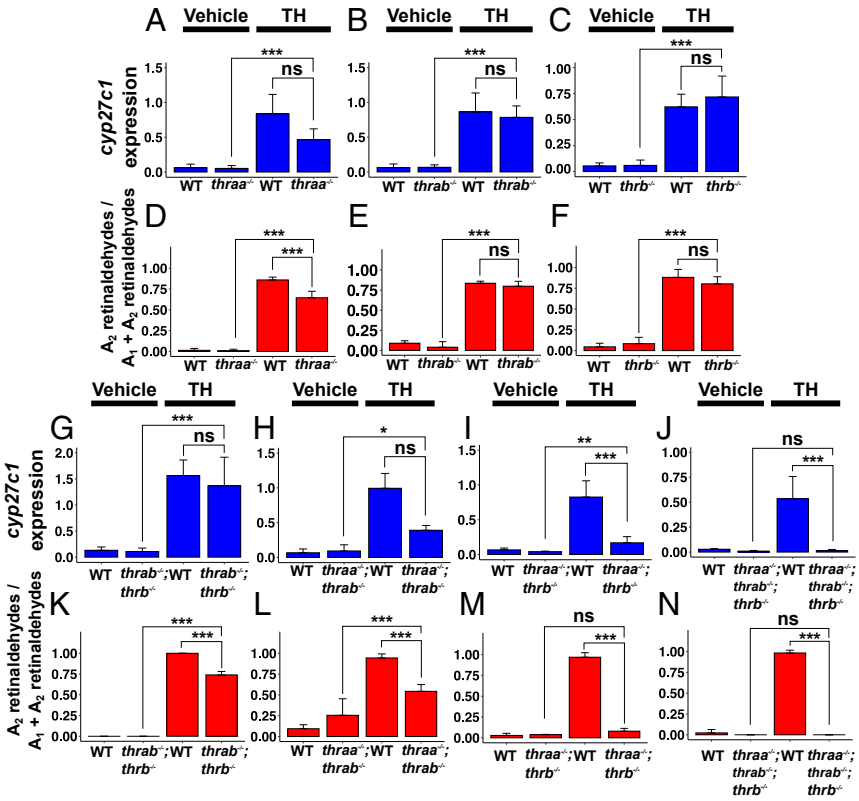

Fig. 2. All three TH receptors contribute to TH-mediated induction of *cyp27c1* expression and the vitamin A_1-to-A_2 shift. Adult (>2 mo old) WT and TH receptor mutants were treated with either vehicle or TH (300 μg/L L-thyroxine) for 3 wk and then harvested for analysis by qPCR (*cyp27c1* expression) and HPLC (vitamin A_2 retinaldehyde production). (*A–F*) TH-induced expression of *cyp27c1* (normalized to *rpl13a* expression [2^{-dCt}]; mean ± SD) and production of vitamin A_2 retinoids are maintained in all three TH receptor mutants, but A_2 levels are modestly reduced in TH-treated *thraa*$^{-/-}$ compared to vehicle-treated. (*G–J*) Induction of *cyp27c1* expression is attenuated in *thraa*$^{-/-}$;*thrb*$^{-/-}$ double mutants and completely lost in *thraa*$^{-/-}$;*thrab*$^{-/-}$;*thrb*$^{-/-}$ fish. (*K–N*) TH-induced vitamin A_2 production is reduced in *thrab*$^{-/-}$;*thrb*$^{-/-}$ and *thraa*$^{-/-}$;*thrab*$^{-/-}$ mutants and eliminated in both *thraa*$^{-/-}$;*thrb*$^{-/-}$ and *thraa*$^{-/-}$;*thrab*$^{-/-}$;*thrb*$^{-/-}$ fish. *thrb*$^{-/-}$ = *thrb*$^{stl627/stl627}$ in all experiments. $n \geq 3$ zebrafish per experimental group. qPCR results were evaluated by one-way ANOVA (F test) followed by a Tukey's honest statistical difference (HSD) test to assess pairwise differences. A_2 data were analyzed within a beta regression framework, in which differences across treatments and genotypes were evaluated using a likelihood ratio test followed by a Tukey's HSD test to assess pairwise differences. ***adjusted $P <$ 0.001; **adjusted $P < 0.01$; *adjusted $P < 0.05$; ns, not significant.

and adult stages. First, we examined larvae at 3 d postfertilization (dpf) using an antibody targeting red cone opsin. We found a complete absence of staining in *thrb*$^{-/-}$ retinas (Fig. 3 *A* and *B*). To determine whether the absence of red cone opsin immunoreactivity is due to loss of opsin expression or an absence of red cones, we used anti-Arr3a, an antibody which labels both green and red cones, to quantify the number of Arr3a^{+} cells in clutch-matched WT and *thrb*$^{-/-}$ retinas at 5 dpf (24). We found that the number of Arr3a^{+} cells is reduced in the *thrb*$^{-/-}$ retina by ∼59% (Fig. 3 *C–E*). The magnitude of this decrease is consistent with the loss of red cones, since the ratio of red to green cones in the larval zebrafish retina is ∼56:44 (25).

Next, we examined the effects of the *thrb* mutation on adult retina. In the WT retina, cone photoreceptors of adult zebrafish are arranged in a "row mosaic" array in which double rows of red and green cones alternate with single rows of UV and blue cones (see "flatmount" in Fig. 1*A*) (25). Thus, by combining antibody staining for Arr3a (red and green cones), Arr3b (blue and UV cones), and DAPI (to highlight relative nuclear position) we were able to unambiguously identify each cone subtype in the adult zebrafish retina. In WT retinas there is a double row of Arr3a^{+} cells, consistent with the presence of two rows of alternating red and green cones (Fig. 3*F*). In contrast, in *thrb*$^{-/-}$ retinas we observed only a single row of Arr3a^{+} cells (Fig. 3*J*). Consistent with this finding, and similar to what we had observed in the larval retina, we found that the number of Arr3a^{+} cells was reduced by approximately half in the adult *thrb*$^{-/-}$ retina (28.6 ± 5.3 cells per 1,600 μm^2) compared to WT (53.8 ± 3.6 cells per 1,600 μm^2) (Fig. 3*N*). In contrast, the number of Arr3b^{+} cells was unchanged in the *thrb*$^{-/-}$ retina (Fig. 3*O*). Costaining with anti-Arr3a and anti-green cone opsin revealed that all Arr3a^{+} cells in the *thrb*$^{-/-}$ retina are green cone opsin^{+}, implying an absence of red cones (Fig. 3*Q*). Despite the deficiency of red cones, the overall arrangement of the photoreceptor array is preserved in the *thrb*$^{-/-}$ retina (compare Fig. 3 *I–M*). This finding contrasts with the reported disruption of the cone photoreceptor mosaic in retinas lacking UV cones (26).

To evaluate the role of *thrb* in cone function, we made ex vivo transretinal electroretinogram (ERG) recordings from adult *thrb*$^{-/-}$ zebrafish retina and age-matched WT controls. First, we isolated the cone component of the flash response by exposing the retinas to a background light that would desensitize the rods and suppress their flash responses (Fig. 4*A*). Next, we measured the sensitivity of cones to flash stimuli of 400-, 500-, 540-, 580-, 600-, 620-, and 640-nm test flashes. We found that the sensitivity of *thrb*$^{-/-}$ retinas was similar to that of WT controls for blue and green wavelengths (i.e., 400, 500, and 540 nm). However, at wavelengths >540 nm, the sensitivity of *thrb*$^{-/-}$ retina declined rapidly, while the sensitivity of WT retinas remained stable (Fig. 4*B*). This result is consistent with a selective loss of red cones in the *thrb*$^{-/-}$ retina.

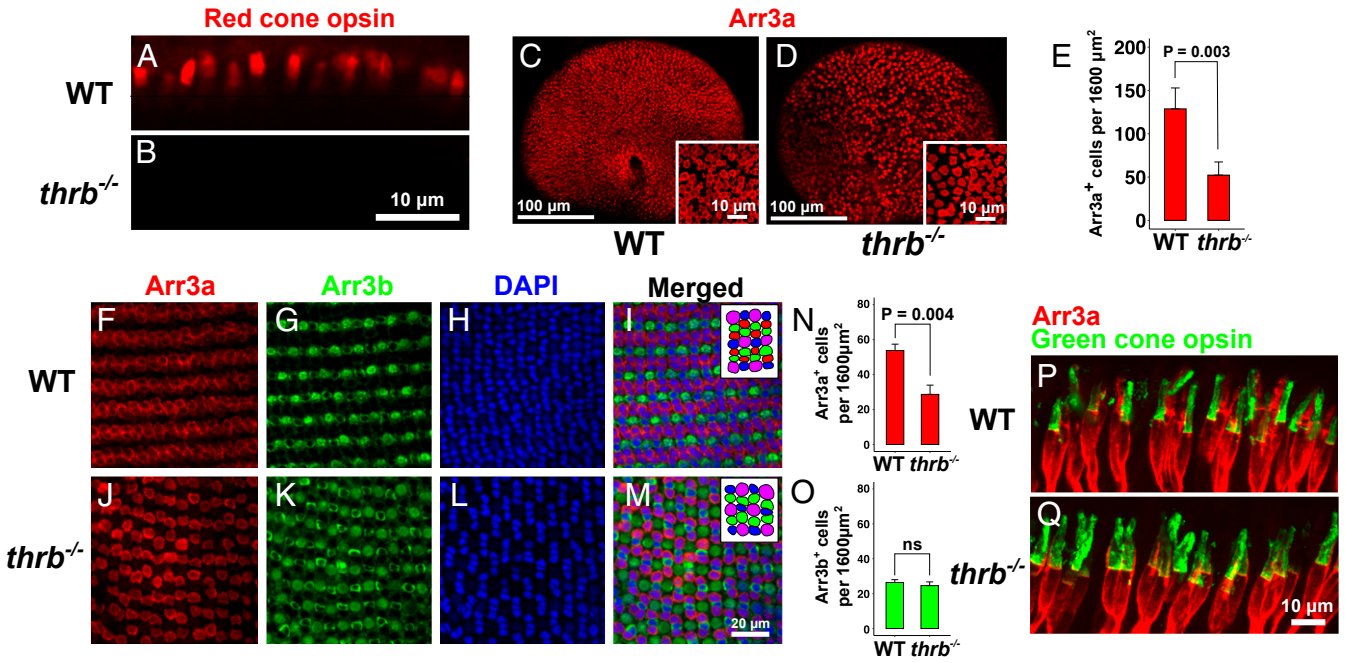

Fig. 3. Red cones are absent from larval and adult *thrb*$^{-/-}$ retina. (*A* and *B*) Images of outer segments of 3 dpf larvae demonstrate a lack of red cone opsin^{+} cells in the 3 dpf *thrb*$^{-/-}$ retina. (*C* and *D*) Wholemount views of 5 dpf WT and *thrb*$^{-/-}$ retina stained with Arr3a antibody demonstrate a reduction in Arr3a^{+} cells in *thrb*$^{-/-}$ retina. *Insets* are high-resolution images taken immediately dorsal to the optic nerve of separate clutch-matched larvae. (*E*) The number of Arr3a cells in the 5 dpf *thrb*$^{-/-}$ retina is reduced relative to WT (mean ± SD; $n = 4$ per group). (*F–M*) Flatmount images of adult 5-mo-old WT and *thrb*$^{-/-}$ retina stained with anti-Arr3a antibody (red and green cones), anti-Arr3b antibody (blue and UV cones), and DAPI (nuclei). (*F* and *J*) The double row of Arr3a^{+} cells in the WT retina is replaced with a single row in the *thrb*$^{-/-}$ retina. (*I* and *M*) Combined images indicate that the patterning of the cone mosaic remains largely intact in the *thrb*$^{-/-}$ retina. (*N*) Quantification of the number of Arr3a^{+} cells in the adult WT and *thrb*$^{-/-}$ retina (mean ± SD; $n = 3$ per group) reveals that the total number of Arr3a^{+} cells is reduced by about half in the *thrb*$^{-/-}$ retina. (*O*) Quantification of the number of Arr3b^{+} cells in the adult WT and *thrb*$^{-/-}$ retina (mean ± SD; $n = 3$ per group) reveals that the number of Arr3b^{+} cells is unchanged. The reduction in the number of Arr3a^{+} cells in the *thrb*$^{-/-}$ retina suggests that either red or green cones are absent. (*P* and *Q*) Sections of adult WT and *thrb*$^{-/-}$ retina (inner and outer segments shown) stained with anti-Arr3a and anti-green cone opsin antibodies. In the WT retina, Arr3a^{+};green cone opsin^{+} cells (green cones) and Arr3a^{+};green cone opsin^{-} cells (red cones) are present. In the *thrb*$^{-/-}$ retina, only Arr3a^{+};green cone opsin^{+} cells (green cones) are present, suggesting red cones are absent. All statistical analyses were performed using two-tailed *t* tests. *thrb*$^{-/-}$ = *thrb*$^{stl627/stl627}$ in *A–O*. *thrb*$^{-/-}$ = *thrb*$^{stl628/stl628}$ in *P* and *Q*. ns, not significant.

We next used RNA-seq to compare the transcriptome of the adult *thrb*$^{-/-}$ retina to that of WT fish. In addition to *thrb* itself, we identify only five down-regulated genes (Fig. 5*A* and Dataset S1). Three of these genes reside in a single syntenic cluster and encode the two paralogous red cone opsins (*lws1* and *lws2*) and a microRNA (*miR-726*) (Fig. 5*B*). A homolog of this microRNA, which is of unknown function, was previously reported to be red cone-specific in medaka (*Oryzias latipes*) (27). Down-regulation of *thrb, lws1*, and *lws2* in *thrb*$^{-/-}$ retina was additionally confirmed by qPCR (*SI Appendix*, Fig. S3). Examination of the distribution of RNA-seq reads at the *lws1/lws2/miR-726* locus indicates that the transcription of the immediately adjacent blue cone opsin gene (*sws2*) is unaffected by the *thrb* mutation (Fig. 5*B*).

Two other genes were found to be down-regulated in *thrb*$^{-/-}$ retina: *si:busm1-57f23.1* and *mhc1uba* (Fig. 5*A*). The former is selectively expressed in developing eye and notochord and encodes a protein with similarity to the mammalian cysteine protease inhibitor cystatin (28). The expression pattern of *mhc1uba*, which encodes a component of the major histocompatibility complex, is less specific but includes the eye and other parts of the developing head (29). Only a single gene, of unknown function (*serinc2*), was found to be modestly up-regulated in *thrb*$^{-/-}$ retina (Fig. 5*A*). Taken together, these findings indicate the presence of only very few red cone-specific genes in adult zebrafish. However, RNA-seq performed on whole retina may limit our ability to detect lowly expressed red cone-specific transcripts or those that are not exclusively red cone-specific.

Next, we conducted a preliminary evaluation of the distribution of cone photoreceptors in adult *thraa*$^{-/-}$ and *thrab*$^{-/-}$ retinas. Staining with anti-Arr3a, anti-Arr3b, and the nuclear marker DRAQ5, revealed a typical photoreceptor nuclear arrangement with a double row of Arr3a^{+} cells and a single row of Arr3b^{+} cells in both mutants (*SI Appendix*, Fig. S4). These results suggest the presence of a normal complement of the four cone photoreceptor subtypes. Given the broad expression pattern of *thraa* and *thrab* in multiple retinal layers (Fig. 1*C*), more subtle effects of these mutations on zebrafish retinal development may exist and will be the subject of future analyses.

Red Cone Precursors Are Transfated into UV Cones and Horizontal Cells in the *thrb*$^{-/-}$ Retina. Morpholino-based knockdown of *thrb* in zebrafish larvae results in both a loss of red cone opsin^{+} cells and a corresponding increase in UV cone opsin^{+} cells (16). One possible explanation for this result is that red cone precursors are transfated into UV cones in the absence of *thrb*. To evaluate this possibility, we examined zebrafish carrying the *trβ2:tdTomato* transgene, which consists of the tdTomato gene under control of the zebrafish *thrb* promoter (16). In these fish, tdTomato is first detected at 2 dpf in precursors that give rise to red cones, horizontal cells, and retinal ganglion cells (16). In WT retina at 3 dpf, we detected tdTomato exclusively in red cones (red cone opsin^{+} cells) in the ONL (Fig. 6*A*). In contrast, in *thrb*$^{-/-}$ retinas, tdTomato^{+} cells occur both in the ONL and in the outermost part of the INL in a distribution similar to that of developing horizontal cells (30) (Fig. 6*B*). The tdTomato^{+} cells in the ONL

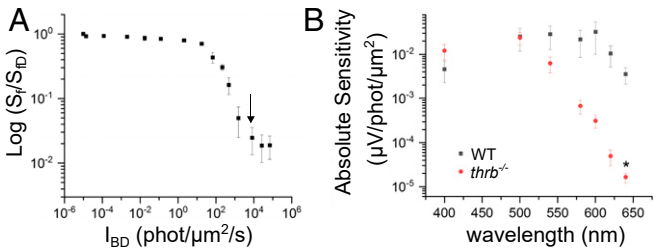

Fig. 4. Adult *thrb*$^{-/-}$ fish exhibit diminished spectral sensitivity at long wavelengths. (*A*) Background light adaptation experiment used to determine the optimal background light intensity for saturating the rods and isolating the cone component of the retina response. Fractional flash sensitivity (S_f) measured by transretinal ERG recordings from WT zebrafish in 460-nm background light of increasing intensity, plotted normalized to the corresponding fractional flash sensitivity in darkness (S_{fD}). The initial gradual decline in dimmer backgrounds is driven by the light adaptation of the rods. Rod sensitivity declines steadily until a plateau is reached. Beyond this point, rod sensitivity becomes lower than cone sensitivity and the overall response from the retina is driven by the cones. We used the background intensity near the beginning of the plateau (8,109 phot/μm^2/s; arrow) to suppress the rod responses and obtain transretinal ERG recordings of cone spectral sensitivity. (*B*) Absolute spectral sensitivity of cones obtained by transretinal ERG recordings in the background light identified in *A*. *thrb*$^{-/-}$ fish (red circles; $n = 9$) lacked the long-wavelength spectral sensitivity (mean ± SEM) observed in WT fish (black squares; $n = 8$). The difference in the absolute spectral sensitivity between the two groups was found to be statistically significant at 640 nm, indicating compromised red cone function in the *thrb*$^{-/-}$ fish. All statistical analyses were performed using two-tailed *t* tests. *$P < 0.05$. *thrb*$^{-/-}$ = *thrb*$^{stl627/stl627}$. Phot, photons.

of *thrb*$^{-/-}$ retinas lack both red cone opsin expression and the presynaptic axonal narrowing seen in tdTomato$^+$ cells in WT retinas (Fig. 6 *A* and *B*). Furthermore, tdTomato$^+$ cells in *thrb*$^{-/-}$ retinas do not express Arr3a, a marker of mature red and green cones (Fig. 6*D*). We note that in the 3 dpf WT retina, Arr3a labeling is primarily in tdTomato$^+$ red cones (Fig. 6*C*), which differs from the pattern of Arr3a expression in the adult retina in which both red and green cones are labeled (Fig. 3*P*). This suggests that the expression of Arr3a in WT fish is delayed in green cones relative to red cones at 3 dpf, consistent with dim Arr3a expression in green cones relative to red cones previously observed at 4 dpf (31). Therefore, the lack of Arr3a expression in tdTomato$^+$ cells in the *thrb*$^{-/-}$ retina at 3 dpf suggests tdTomato$^+$ precursors are transfated into a nonred cone (Arr3a$^-$) photoreceptor subtype and that the remaining Arr3a$^+$ cells represent green cones in which Arr3a expression appears to be accelerated (Fig. 6*D*). Overall, our results in Fig. 6 *B* and *D* suggest that in the absence of *thrb*, tdTomato$^+$ precursors are transfated into a nonred/nongreen photoreceptor subtype and into cells that resemble horizontal cells.

To evaluate the possibility that tdTomato$^+$ precursors in the *thrb*$^{-/-}$ retina are transfated into UV cones, we used antibody staining to compare the number of UV cone opsin$^+$ cells in WT and *thrb*$^{-/-}$ retinas at 3 dpf. We found a significant increase in the number of UV cone opsin$^+$ cells in *thrb*$^{-/-}$ retinas compared to WT (Fig. 6*F*). Application of the UV cone opsin antibody to WT and *thrb*$^{-/-}$ fish carrying the *trβ2:tdTomato* transgene confirmed that a large subset of *trβ2:tdTomato*$^+$ precursors are transfated into UV cone opsin$^+$ cells (closed arrow in Fig. 6 *E* and *G*). We also observed a second population of UV cone opsin$^+$ cells in the *thrb*$^{-/-}$ retina which are tdTomato$^-$; these cells likely represent native UV cones (open arrow in Fig. 6*E*). In further confirmation of these results, we observed that nearly all *trβ2:tdTomato*$^+$ cells in the ONL of the *thrb*$^{-/-}$ retina are positive for the *sws1:GFP* transgene which exclusively marks UV cones (Fig. 6 *I–K*) (32). The latter finding suggests that *trβ2:tdTomato*$^+$ cells in the *thrb*$^{-/-}$ retina are exclusively converted into UV cones and not other photoreceptor subtypes within the ONL.

In addition to these findings, we observed that ∼32% (mean ± 0.04 SD, $n = 5$) of tdTomato$^+$ cells in the larval *thrb*$^{-/-}$ retina reside in the INL (asterisk in Fig. 6*B*). In contrast, we never observed tdTomato$^+$ cells in the INL of WT retina (Fig. 6*H*). The localization of these tdTomato$^+$ cells at the outer edge of the INL suggested that they might be horizontal cells. Indeed, we found that tdTomato expression in the INL colocalizes with expression of the *ptf1a:GFP* transgene, a marker of horizontal cells (Fig. 6 *L–N*) (30). These cells may represent new horizontal cells derived from cells originally fated to be red cones. Alternatively, it is possible that these cells are normal horizontal cells with aberrantly perdurant tdTomato expression.

In order to determine if transfating of *trβ2:tdTomato*$^+$ red cone precursors to UV cones also occurs in the growing retina of mature *thrb*$^{-/-}$ fish, we analyzed coexpression of the UV cone-specific *sws1:GFP*$^+$ transgene and *trβ2:tdTomato*$^+$ near the ciliary marginal zone (CMZ) of 12 dpf zebrafish. We find that multiple *thrb:tdTomato*$^+$ cells colocalize with *sws1:GFP* near the *thrb*$^{-/-}$ CMZ, suggesting that red cone precursors are transfated to UV cones when new retina is added during zebrafish growth (Fig. 6 *O–U*). Despite the presence of these double-positive cells, we observed no evidence of supernumerary UV cones within the cone mosaic of adult *thrb*$^{-/-}$ fish (Fig. 3 *K* and *O*). We speculate

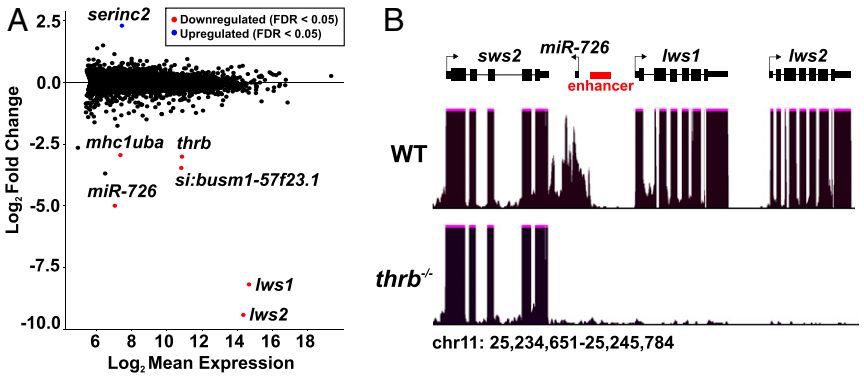

Fig. 5. Expression of only a very small number of genes is dysregulated in adult *thrb*$^{-/-}$ retina. (*A*) Plot comparing gene expression in 6-mo-old WT and *thrb*$^{-/-}$ retina obtained via RNA-seq (WT $n = 3$, *thrb*$^{-/-}$ $n = 3$). Only five genes (excluding *thrb*) are significantly down-regulated in the *thrb*$^{-/-}$ retina. *miR-726*, *lws1*, and *lws2* are previously characterized red-cone-specific genes. *mhc1uba* and *si:busm1-57f23.1* are putative red cone-enriched genes. (*B*) Screenshots of University of California Santa Cruz genome browser tracks demonstrate a selective loss of transcripts corresponding to *lws1*, *lws2*, and *miR-726*, and a normal number of transcripts corresponding to blue cone opsin (*sws2*). The enhancer labeled in red was previously shown to coordinately regulate *lws1* and *lws2* in zebrafish (4). In medaka, the orthologous enhancer regulates *miR-726* and *LWS-A*, the single medaka ortholog of *lws1/2* (27). *thrb*$^{-/-}$ = *thrb*$^{stl628/stl628}$. FDR, false discovery rate (adjusted *P* value).

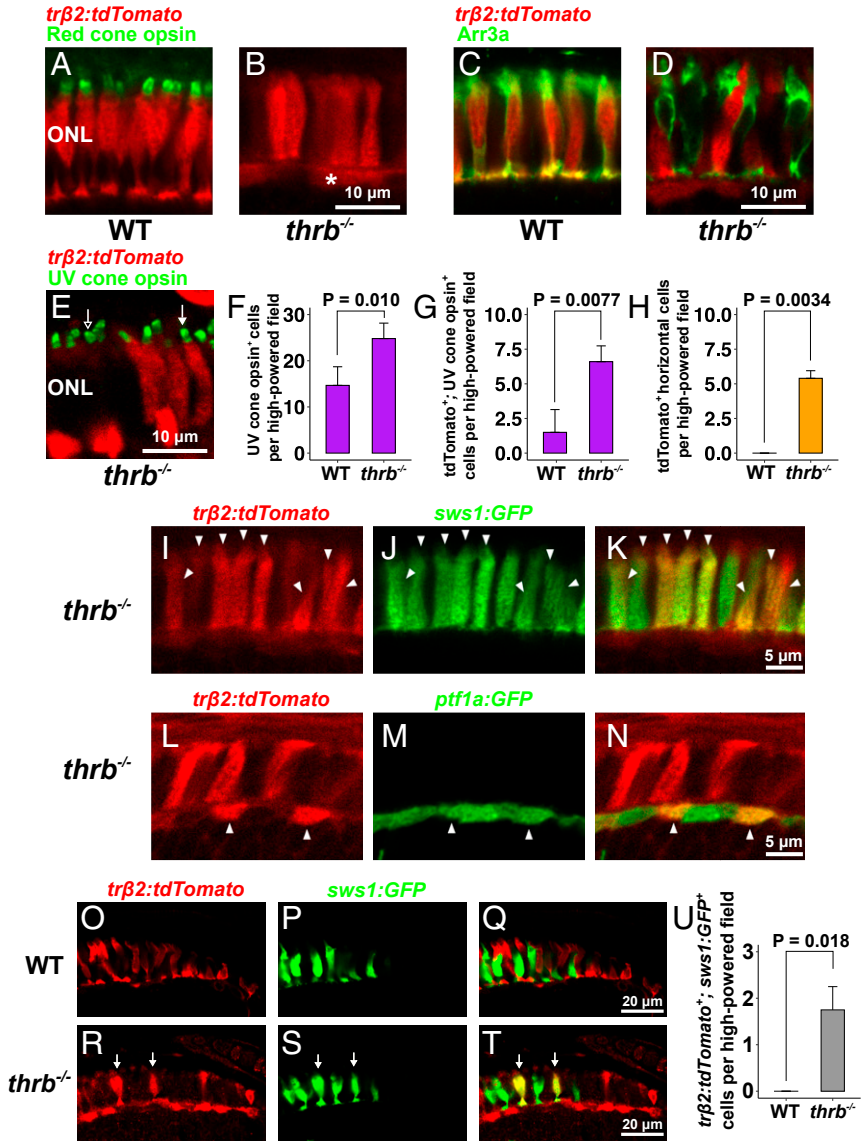

Fig. 6. Red cone precursors are transfated into UV cones in the larval and CMZ-derived *thrb*$^{-/-}$ retina. (*A–D*) Optical sections of the ONL of 3 dpf *trβ2:tdTomato*$^{+}$ and *trβ2:tdTomato*$^{+}$;*thrb*$^{-/-}$ larvae. (*A* and *B*) In the *thrb*$^{-/-}$ retina, *trβ2:tdTomato*$^{+}$ cells that reside in the ONL lack red cone opsin expression. Those cells that reside in the outermost INL resemble developing horizontal cells (asterisk). (*C* and *D*) In the *thrb*$^{-/-}$ retina, *trβ2:tdTomato*$^{+}$ cells do not express Arr3a ($n = 4$ WT, $n = 5$ *thrb*$^{-/-}$). (*E*) Confocal projection image of the ONL of 3 dpf *trβ2:tdTomato*$^{+}$;*thrb*$^{-/-}$ larvae shows that the majority of *trβ2:tdTomato*$^{+}$ cells in the ONL are UV cone opsin^{+} (closed arrow). UV cone opsin^{+} cells that are *trβ2:tdTomato*$^{-}$ (open arrow) are likely native UV cones. (*F–H*) Quantification of cell populations in the 3 dpf WT and *thrb*$^{-/-}$ retina across 76 μm (mean ± SD, $n = 6$ WT, $n = 5$ *thrb*$^{-/-}$). (*F*) The number of UV cones is increased in the *thrb*$^{-/-}$ retina. (*G*) The number of *trβ2:tdTomato*$^{+}$;UV cone opsin^{+} cells is increased in the *thrb*$^{-/-}$ retina, suggesting that *trβ2:tdTomato*$^{+}$ red cone precursors are transfated into UV cones in the *thrb*$^{-/-}$ background. (*H*) The number of *trβ2:tdTomato*$^{+}$ cells in the outer part of the INL (confirmed to be *ptf1a:GFP*$^{+}$ horizontal cells in *L–N*) is increased in *thrb*$^{-/-}$ retinas, suggesting that a subset of *trβ2:tdTomato*$^{+}$ red cone precursors have been transfated into horizontal cells. (*I–N*) Optical sections of the retina of 3 dpf *trβ2:tdTomato*$^{+}$;*thrb*$^{-/-}$ larvae. (*I–K*) Almost all *trβ2:tdTomato*$^{+}$ cells that reside in the ONL colocalize with *sws1:GFP* (arrowheads) and are therefore transfated to UV cones ($n = 3$ retinas). (*L–N*) *trβ2:tdTomato*$^{+}$ cells in the INL colocalize with *ptf1a:GFP* (arrowheads), suggesting that they may represent transfated horizontal cells. ($n = 4$ retinas). (*O–U*) Red cone precursors are transfated into UV cones in the CMZ-derived *thrb*$^{-/-}$ retina (*O–T*). Optical sections of the ONL immediately adjacent to the temporal CMZ of 12 dpf *trβ2:tdTomato*$^{+}$ and *trβ2:tdTomato*$^{+}$;*thrb*$^{-/-}$ retina, tdTomato stained with anti-tdTomato antibody (*O–Q*). In the WT retina, the *sws1:GFP* transgene is not expressed in *trβ2:tdTomato*$^{+}$ cells (*R–T*). In the *thrb*$^{-/-}$ retina, a subset of *trβ2:tdTomato*$^{+}$ cells are *sws1:GFP*$^{+}$ (arrows), suggesting red cone precursors are transfated to *sws1:GFP*$^{+}$ UV cones. The *sws1:GFP*$^{+}$ cells that are *trβ2:tdTomato*$^{-}$ are likely native UV cones. (*U*) The number of *trβ2:tdTomato*$^{+}$; *sws1:GFP*$^{+}$ cells across 94 μm immediately adjacent to the CMZ is increased in the 12 dpf *thrb*$^{-/-}$ retina (mean ± SD, $n = 4$/group). All statistical tests were performed using Mann–Whitney *U* test. *thrb*$^{-/-}$ = *thrb*$^{stl627/stl627}$.

that transfated UV cones derived from adult CMZ die prior to formation of the adult mosaic.

Discussion

TH nuclear receptors play a crucial role in at least two aspects of long-wavelength vision in zebrafish: determination of red cone fate and control of *cyp27c1* expression. Here, we show that in the retina, *thrb* regulates the fate of red cone precursors, which in the absence of *thrb* transdifferentiate into UV cones and horizontal cells. We also show that in the RPE, TH acts through all three TH receptors (*thraa*, *thrab*, and *thrb*) to regulate *cyp27c1* expression and the resulting production of vitamin A_2-based retinoids. Recent

studies indicate that TH signaling also enhances expression of red-shifted paralogs of green and red cone opsin in both salmonids and zebrafish (14, 15). Thus, TH signaling coordinates multiple aspects of long-wavelength vision.

Comparison of the transcriptomes of WT and *thrb*$^{-/-}$ retinas revealed only five down-regulated genes, suggesting the existence of very few red cone-specific genes. This finding contrasts with the discovery of hundreds of differentially expressed genes between cone subtypes in developing chicken retina (33). The greater degree of transcriptomic divergence between avian cone subtypes might be attributable to the greater number of structural differences between subtypes, including the presence/absence of intracellular organelles such as oil droplets and paraboloids (34, 35). Additionally, avian cone subtypes show differences in oil droplet pigmentation which is mediated by the differential expression of carotenoid-metabolizing enzymes and transporters (34, 36, 37). An alternative interpretation of our findings is that analysis of whole retina (rather than sorted cone subtypes) may have limited our ability to detect red cone-specific genes. Clearly, further studies will be required to determine the full extent of transcriptome divergence between zebrafish cone subtypes.

The transfating of red cone precursors to UV cones in the *thrb*$^{-/-}$ zebrafish retina suggests that *thrb* may have a similarly conserved developmental role in other vertebrate species. Studies in mouse have shown that in the *Thrb2*$^{-/-}$ retina, *Opn1mw* (orthologous to zebrafish *lws1/2*) expression is reduced and *Opn1sw* (orthologous to zebrafish *sws1*) expression is increased (17). These results could be explained in part by a transfating event similar to that observed in *thrb*$^{-/-}$ zebrafish retina. Although we observe transfating to UV cones in both embryo-derived and CMZ-derived *thrb*$^{-/-}$ retina, supernumerary UV cones are not detected in the definitive adult mosaic, suggesting that transfated UV cones die soon after birth. By comparing the transcriptome of native and transfated UV cones, we might discover novel factors required for the viability of native UV cones.

TH has long been known as a potent physiological regulator. For example, it plays a major role in amphibian metamorphosis and in the induction of physiological changes associated with the parr-to-smolt transition of migratory salmon (38–40). Many of these TH-induced changes serve to promote adaptation to new environments (38–40). Although nothing is known about how TH regulates the A_1-to-A_2 switch in wild zebrafish, our work suggests that TH receptors may regulate *cyp27c1* expression under natural conditions. For example, day length or water temperature may influence *cyp27c1* expression in wild zebrafish, as these environmental factors have been shown to regulate the A_1-to-A_2 switch in other aquatic vertebrates (7).

In summary, we have found that TH receptors regulate two aspects of long-wavelength vision via the control of cone development and chromophore usage. The present study expands our understanding of the transcriptional mechanisms underlying these processes and suggests a coordinated mechanism by which TH facilitates visual system adaptation to red-shifted photic environments.

Materials and Methods

Mutant Zebrafish and Transgenic Lines. All procedures were carried out in accordance with the animal protocol approved by the Animal Studies Committee of Washington University. The *albino* line (*alb*$^{b4/b4}$) was used for ISH experiments (20). The *Tg(trβ2:tdTomato)* transgenic line was a generous gift from Rachel Wong (University of Washington, Seattle, WA) (16). The *Tg(ptf1a:GFP)* transgenic line was a generous gift from Ryan Anderson (Indiana University School of Medicine, Indianapolis, IN) (30). The *Tg(sws1:GFP)* transgenic line, *Tg*(zfSWS1-5.5A:EGFP)^{tkk002}, was acquired from the Zebrafish National BioResource Project (https://shigen.nig.ac.jp/zebra/) (32). The *thraa*^{vp33rc1} and *thrab*^{vp31rc1} lines have been previously described in ref. 22. The *thrb*^{stl627} and *thrb*^{stl628} alleles were generated in-house using CRISPR-Cas9 with gRNAs targeting exon 9 of *thrb*. Further details are described in *SI Appendix, Materials and Methods*.

In Situ Hybridization. Anti-sense probes were prepared for *thraa*, *thrab*, *thrb*, and *rpe65a*. Detailed information is provided in *SI Appendix, Materials and Methods*.

Quantitative RT-PCR. WT and mutant fish were treated with TH (750 μL 400 μg/mL L-thyroxine in 0.1 M NaOH per liter of water for a final concentration of 300 μg/L) or vehicle control (750 μL of 0.1 M NaOH per liter of water), and *cyp27c1* expression was quantified using RNA extracted from eyes after removal of the lens. The expression of *thraa*, *thrab*, and *thrb* was quantified using RNA extracted from dissected retina and RPE. Further details are described in *SI Appendix, Materials and Methods*.

Antibodies and Immunohistochemistry. Primary antibodies used were as follows: rabbit polyclonal anti-DsRed (1:200; 632496, TakaraBio), which recognizes tdTomato (16); mouse monoclonal zpr1 (1:50; Zebrafish International Resource Center), which recognizes Arr3a (41, 42); rat monoclonal 10C9.1 (1:50, gift from Ted Allison, University of Alberta, Edmonton, Alberta, Canada), which recognizes UV cone opsin (43); mouse monoclonal 1D4 (1:50, AB5417, Abcam), which recognizes red cone opsin (44); chicken polyclonal anti-Arr3b (24) (1:250; gift from Stephan Neuhauss, University of Zurich, Zurich, Switzerland); and rabbit polyclonal anti-green cone opsin (45) (1:500, gift from David Hyde, University of Notre Dame, Notre Dame, IN). Secondary antibodies were as follows: donkey polyclonal anti-rat IgG conjugated with Alexa-488 (1:200, A21208, Invitrogen); goat polyclonal anti-mouse IgG conjugated with Alexa-488 (1:200, A11029, Invitrogen); goat polyclonal anti-chicken IgY conjugated with Alexa-488 (1:200; A11039, Invitrogen); donkey polyclonal anti-rabbit IgG conjugated with Alexa-488 (1:500; A21206, Invitrogen); donkey polyclonal anti-rabbit IgG conjugated with Alexa-555 (1:1,000; A31572, Invitrogen); and donkey polyclonal anti-mouse IgG antibody conjugated with Alexa-555 (1:200; A31570, Invitrogen). Further details on immunostaining are described in *SI Appendix, Materials and Methods*.

High Performance Liquid Chromatography. Whole eyes from vehicle and TH-treated WT and mutant zebrafish were collected and homogenized. Retinaldehydes were then derivatized to oximes using hydroxylamine treatment (Sigma, 255580). The quantities of A_1- and A_2-based retinaldehydes were then calculated based on all-*trans*-retinaldehyde oxime standards. Additional details are provided in *SI Appendix, Materials and Methods*.

RNA-Seq. For RNA-seq, 6 mo old WT and clutch-matched *thrb*$^{stl628/stl628}$ zebrafish retina were isolated. Two retinas from a male and two retinas from a female zebrafish were combined to make one sample. Three WT and *thrb*$^{stl628/stl628}$ samples were collected and RNA was extracted. Further details regarding RNA extraction, library preparation, sequencing, and data analysis are provided in *SI Appendix, Materials and Methods*.

Data Availability. RNA-seq data are available under GEO accession number GSE143312 (46). Analysis of differentially expressed genes in adult WT and *thrb*$^{stl628/stl628}$ retina is available in Dataset S1.

ACKNOWLEDGMENTS. We thank Rachel Wong for providing the *Tg(trβ2:tdTomato)* zebrafish line, Ryan Anderson for providing the *Tg(ptf1a:GFP)* zebrafish line, Shoji Kawamura for providing the *Tg(sws1:GFP)* zebrafish line, Stephan Neuhauss for the anti-Arr3b antibody, Ted Allison for the anti-UV cone opsin antibody, David Hyde for the anti-green cone opsin antibody, and Michael Nonet for Cas9 protein. We thank Matthew Toomey for assistance with HPLC analysis and Dan Murphy for assistance with bioinformatic analysis. We thank Sam Meiselman and George Johnson for conducting prelimary experiments. We thank Yohei Ogawa, Kyla Serres, Connie Myers, and Nathan Mundell for critical feedback on the project and the manuscript. This work was supported by the National Institutes of Health (EY024958, EY025196, and EY026672 to J.C.C.; EY025696 and EY027387 to V.J.K.; and GM122471 to D.M.P.).

1. S. Yokoyama, H. Yang, W. T. Starmer, Molecular basis of spectral tuning in the red- and green-sensitive (M/LWS) pigments in vertebrates. *Genetics* **179**, 2037–2043 (2008).
2. A. Terakita, The opsins. *Genome Biol.* **6**, 213 (2005).
3. Y. Shichida, T. Matsuyama, Evolution of opsins and phototransduction. *Philos. Trans. R Soc. Lond. B Biol. Sci.* **364**, 2881–2895 (2009).
4. T. Tsujimura, T. Hosoya, S. Kawamura, A single enhancer regulating the differential expression of duplicated red-sensitive opsin genes in zebrafish. *PLoS Genet.* **6**, e1001245 (2010).
5. T. Tsujimura, R. Masuda, R. Ashino, S. Kawamura, Spatially differentiated expression of quadruplicated green-sensitive RH2 opsin genes in zebrafish is determined by proximal regulatory regions and gene order to the locus control region. *BMC Genet.* **16**, 130 (2015).

6. C. D. B. Bridges, Storage, distribution and utilization of vitamins A in the eyes of adult amphibians and their tadpoles. *Vision Res.* **15**, 1311–1323 (1975).
7. D. D. Beatty, Visual pigments and the labile scotopic visual system of fish. *Vision Res.* **24**, 1563–1573 (1984).
8. G. Wald, The metamorphosis of visual systems in the sea lamprey. *J. Gen. Physiol.* **40**, 901–914 (1957).
9. A. Morshedian *et al*., Cambrian origin of the CYP27C1-mediated vitamin A_1-to-A_2 switch, a key mechanism of vertebrate sensory plasticity. *R. Soc. Open Sci.* **4**, 170362 (2017).
10. C. D. B. Bridges, "The Rhodopsin-Porphyropsin Visual System" in *Handbook of Sensory Physiology*, (Springer-Verlag, Berlin, 1972), Vol. VII, pp. 417–480.
11. J. M. Enright *et al*., Cyp27c1 red-shifts the spectral sensitivity of photoreceptors by converting Vitamin A_1 into A_2. *Curr. Biol.* **25**, 3048–3057 (2015).
12. W. T. Allison, T. J. Haimberger, C. W. Hawryshyn, S. E. Temple, Visual pigment composition in zebrafish: Evidence for a rhodopsin-porphyropsin interchange system. *Vis. Neurosci.* **21**, 945–952 (2004).
13. K. J. Gan, I. Novales Flamarique, Thyroid hormone accelerates opsin expression during early photoreceptor differentiation and induces opsin switching in differentiated TRα-expressing cones of the salmonid retina. *Dev. Dyn.* **239**, 2700–2713 (2010).
14. S. E. Temple *et al*., Effects of exogenous thyroid hormones on visual pigment composition in coho salmon (Oncorhynchus kisutch). *J. Exp. Biol.* **211**, 2134–2143 (2008).
15. R. D. Mackin *et al*., Endocrine regulation of multichromatic color vision. *Proc. Natl. Acad. Sci. U.S.A.* **116**, 16882–16891 (2019).
16. S. C. Suzuki *et al*., Cone photoreceptor types in zebrafish are generated by symmetric terminal divisions of dedicated precursors. *Proc. Natl. Acad. Sci. U.S.A.* **110**, 15109–15114 (2013).
17. L. Ng *et al*., A thyroid hormone receptor that is required for the development of green cone photoreceptors. *Nat. Genet.* **27**, 94–98 (2001).
18. K. C. Eldred *et al*., Thyroid hormone signaling specifies cone subtypes in human retinal organoids. *Science* **362**, eaau6348 (2018).
19. V. M. Darras, S. L. J. Van Herck, M. Heijlen, B. De Groef, Thyroid hormone receptors in two model species for vertebrate embryonic development: Chicken and zebrafish. *J. Thyroid Res.* **2011**, 402320 (2011).
20. R. N. Kelsh *et al*., Zebrafish pigmentation mutations and the processes of neural crest development. *Development* **123**, 369–389 (1996).
21. T. Hoang *et al*., Cross-species transcriptomic and epigenomic analysis reveals key regulators of injury response and neuronal regeneration in vertebrate retinas. *bioRxiv*, 10.1101/717876 (2019).
22. L. M. Saunders *et al*., Thyroid hormone regulates distinct paths to maturation in pigment cell lineages. *eLife* **8**, 1–29 (2019).
23. D. Y. R. Stainier *et al*., Guidelines for morpholino use in zebrafish. *PLoS Genet.* **13**, e1007000 (2017).
24. S. L. Renninger, M. Gesemann, S. C. Neuhauss, Cone arrestin confers cone vision of high temporal resolution in zebrafish larvae. *Eur. J. Neurosci.* **33**, 658–667 (2011).
25. W. T. Allison *et al*., Ontogeny of cone photoreceptor mosaics in zebrafish. *J. Comp. Neurol.* **518**, 4182–4195 (2010).
26. P. A. Raymond *et al*., Patterning the cone mosaic array in zebrafish retina requires specification of ultraviolet-sensitive cones. *PLoS One* **9**, e85325 (2014).
27. Y. Daido, S. Hamanishi, T. G. Kusakabe, Transcriptional co-regulation of evolutionarily conserved microRNA/cone opsin gene pairs: Implications for photoreceptor subtype specification. *Dev. Biol.* **392**, 117–129 (2014).
28. B. Thisse, C. Thisse, Fast release clones: A high throughput expression analysis. ZFIN Direct Data Submission. https://zfin.org/action/figure/all-figure-view/ZDB-PUB-040907-1?probeZdbID=ZDB-CDNA-050612-86. Accessed November 2019.
29. B. Thisse, C. Thisse, Fast release clones: A high throughput expression analysis. ZFIN Direct Data Submission. https://zfin.org/ZDB-FIG-060216-726. Accessed November 2019.
30. L. Godinho *et al*., Nonapical symmetric divisions underlie horizontal cell layer formation in the developing retina in vivo. *Neuron* **56**, 597–603 (2007).
31. M. Sotolongo-Lopez, K. Alvarez-Delfin, C. J. Saade, D. L. Vera, J. M. Fadool, Genetic dissection of dual roles for the transcription factor six7 in photoreceptor development and patterning in zebrafish. *PLoS Genet.* **12**, e1005968 (2016).
32. M. Takechi, T. Hamaoka, S. Kawamura, Fluorescence visualization of ultraviolet-sensitive cone photoreceptor development in living zebrafish. *FEBS Lett.* **553**, 90–94 (2003).
33. J. M. Enright, K. A. Lawrence, T. Hadzic, J. C. Corbo, Transcriptome profiling of developing photoreceptor subtypes reveals candidate genes involved in avian photoreceptor diversification. *J. Comp. Neurol.* **523**, 649–668 (2015).
34. M. B. Toomey, J. C. Corbo, Evolution, development and function of vertebrate cone oil droplets. *Front. Neural Circuits* **11**, 97 (2017).
35. V. B. Morris, C. D. Shorey, An electron microscope study of types of receptor in the chick retina. *J. Comp. Neurol.* **129**, 313–340 (1967).
36. R. J. Lopes *et al*., Genetic basis for red coloration in birds. *Curr. Biol.* **26**, 1427–1434 (2016).
37. M. B. Toomey *et al*., Complementary shifts in photoreceptor spectral tuning unlock the full adaptive potential of ultraviolet vision in birds. *eLife* **5**, 1–27 (2016).
38. V. Laudet, The origins and evolution of vertebrate metamorphosis. *Curr. Biol.* **21**, R726–R737 (2011).
39. B. T. Björnsson, S. O. Stefansson, S. D. McCormick, Environmental endocrinology of salmon smoltification. *Gen. Comp. Endocrinol.* **170**, 290–298 (2011).
40. K. B. Staley, R. D. Ewing, Purine levels in the skin of juvenile coho salmon (Oncorhynchus kisutch) during parr-smolt transformation and adaptation to seawater. *Comp. Biochem. Physiol. B* **101**, 447–452 (1992).
41. K. E. Ile *et al*., Zebrafish class 1 phosphatidylinositol transfer proteins: PITPbeta and double cone cell outer segment integrity in retina. *Traffic* **11**, 1151–1167 (2010).
42. K. D. Larison, R. Bremiller, Early onset of phenotype and cell patterning in the embryonic zebrafish retina. *Development* **109**, 567–576 (1990).
43. M. G. Duval, A. P. Oel, W. T. Allison, gdf6a is required for cone photoreceptor subtype differentiation and for the actions of tbx2b in determining rod versus cone photoreceptor fate. *PLoS One* **9**, e92991 (2014).
44. J. Yin *et al*., The 1D4 antibody labels outer segments of long double cone but not rod photoreceptors in zebrafish. *Invest. Ophthalmol. Vis. Sci.* **53**, 4943–4951 (2012).
45. T. S. Vihtelic, C. J. Doro, D. R. Hyde, Cloning and characterization of six zebrafish photoreceptor opsin cDNAs and immunolocalization of their corresponding proteins. *Vis. Neurosci.* **16**, 571–585 (1999).
46. L. I. Volkov, J. Kim-Han, L. M. Saunders, D. M. Parichy, J. C. Corbo, Zebrafish Retina thrb-/- RNA-seq. Gene Expression Omnibus. https://www.ncbi.nlm.nih.gov/geo/query/acc.cgi?acc=GSE143312. Deposited 8 January 2020.

PNAS
www.pnas.org

Supplementary Information for

Thyroid hormone receptors mediate two distinct mechanisms of long-wavelength vision

Leo I. Volkov[1], Jeong Sook Kim-Han[2], Lauren M. Saunders[3], Deepak Poria[4], Andrew E.O. Hughes[1], Vladimir J. Kefalov[4], David M. Parichy[3], and Joseph C. Corbo[1,5]

[1]Department of Pathology and Immunology, Washington University School of Medicine, St. Louis, MO; [2]Department of Pharmacology, A.T. Still University of Health Sciences, Kirksville, MO; [3]Department of Biology and Department of Cell Biology, University of Virginia, Charlottesville, VA; [4]Department of Ophthalmology and Visual Sciences, Washington University School of Medicine, St. Louis, MO

[5]corresponding author

Email: jcorbo@wustl.edu

This PDF file includes:

SI Materials and Methods

Figures S1 to S4

Legend for Dataset S1

SI References

Other supplementary materials for this manuscript include the following:

Dataset S1

www.pnas.org/cgi/doi/10.1073/pnas.1920086117

SI Materials and Methods

Zebrafish Husbandry. All procedures were carried out in accordance with an animal protocol approved by the Animal Studies Committee of Washington University in St. Louis. Zebrafish were maintained in the Washington University Zebrafish facility on a 14:10 light: dark cycle at 27° C. Adult fish were fed with Lansy NRD 4/6, Salt Creek Progression 4, and Argent Cylopeze, as well as live *Artemia nauplii*. Wild-type fish represent the AB* strain from Washington University in St. Louis.

Generation of *thrb* mutant zebrafish. Mutant zebrafish were generated using CRISPR-Cas9 technology. The guide RNAs (gRNAs) were designed using online tools CRISPRscan and CRISPOR (1, 2). Three gRNAs, one targeting Exon 6 (GGATGGCCTCATCTTTCCAG) of *thrb* and two targeting exon 9 (GGATGGCCTCATCTTTCCAG and GGAAGAGTGGGAGATGATAC) were ordered from Integrated DNA Technologies, annealed and ligated into the pDR274 vector (3). gRNA templates were synthesized by PCR using forward gRNA amplicon 5'-GTTGGAACCTCTTACGTGCC-3' and reverse gRNA amplicon 5'-AAAAGCACCGACTCGGTG-3' yielding a 369 bp PCR product, which were used for *in vitro* transcription using MegaScript (Ambion). gRNAs was purified by Bio-Spin P30 or LiCl precipitation. Zebrafish embryos were injected at the 1-cell stage with a 1 nl mixture of all three gRNAs mentioned above (100ng/µl), Cas9 protein (800 ng/µl), KCl (300 mM), and phenol red (0.05%). The initial screening was done by PCR using genomic DNA from 1-2 embryos followed by DNA fragment analysis using a single-step PCR with 3-primers (5'-TGTAAAACGACGGCCAGTGGTGTGTTGTGGATAGTTTGTGC-3', 5'-GTGTCTTAGACCTCTCACCAGGAATTTGC-3', and 6FAM-TGTAAAACGACGGCCAGT-3'). Clutches with suspected *thrb* mutants were grown to sexual maturity, outcrossed to AB* wildtypes to isolate heterozygous mutants, then intercrossed to isolate homozygous *thrb* mutants.

Genotyping. Mutant fish were genotyped by PCR. To extract genomic DNA for genotyping adult zebrafish, tail fins were incubated in 100 µl 50 mM NaOH at 95° C for 30 minutes, cooled to 4° C, and then 10 µl of 1 M Tris pH 8.0 was added to the solution. To extract genomic DNA for genotyping larval zebrafish, posterior segments were incubated in 50 µl 50 mM NaOH at 95° C for 10 minutes, cooled to 4° C, and 5 µl of 1 M Tris pH 8.0 was added to the solution. Samples were then diluted 1:10 in water and used for PCR. Mutant fish were genotyped using primers that spanned the mutations such that WT and mutant alleles yielded products of different sizes. The following genotyping primers were used: for *thrb*^{stl627} and *thrb*^{stl628}: 5'-tgtaaaacgacggccagTGGTGTGTTGTGGATAGTTTGTGC-3' and 5'-gtgtcttAGACCTCTCACCAGGAATTTGC-3'; for *thraa*^{vp33rc1}: 5'-CATGTGATGCAGCGGTAATGA-3' and 5'-TGGAGAAAGATGAGCCGTGT-3'; for *thrab*^{vp31rc1}: 5'-AGCTATCTGGAGAAGGATGAGC-3' and 5'-GAAGACCAACCTTACAGCCC-3'.

***In situ* hybridization.** *In situ* hybridization was performed according to Trimarchi et al. (4). Probe templates (400-900 bp) were obtained by PCR from cDNA derived from 2 dpf zebrafish. Primers for TH receptors included *Xho*I sites for forward primers and *Xba*I sites for reverse primers for subsequent cloning into the pBlueScript SK(+) (pBSK+) vector. Primers for *rpe65a* included *Eco*RI sites for cloning into pBSK+, as previously described (5). Primers: *thraa:* 5'-TATACTCGAGAAACCTTCATCCGTCCTATTCCTG-3' and *5'-*AATTTCTAGAAGGTTCGTCACCTTCATCAGC-3', *thrab:* 5'-TATACTCGAGCATGGATTTGGTACTGGACGAC-*3'* and *5'-*AATTTCTAGACACACGTCCTGATCCTCGAAG-3', *thrb:* *5'-*TATACTCGAGAAGTTACCTGGACAAGGATGAGC-3' and *5'-*AATTTCTAGATTGTTTCCAGTGGTTGCCTTG-3', *rpe65a:* 5'-TCCCCGGAATTCAGCTGAACGAACCTCTTCCA-3' and 5'-TCCCCGGAATTCGATGGCTTGAACCTCTCAGC-3'

Template sequence and orientation were verified by Sanger sequencing. DIG-labeled probe synthesis was performed as previously described (4). Probes were used at a concentration

of 1 µl per 100 µl hybridization buffer. Hybridization was performed on 12 µm-thick sections of *albino* zebrafish eyes as previously described (4).

Thyroid Hormone (TH) Treatment. TH treatment was performed as in (5). Briefly, individually housed zebrafish were kept in water containing either thyroid hormone (750 µl 400 µg/ml L-thyroxine in 0.1 M NaOH per liter of water for a final concentration of 300 µg/l) or vehicle control (750 µl of 0.1 M NaOH per liter of water) for three weeks without feeding. Water was replaced every two days.

Quantitative RT-PCR. For analysis of *cyp27c1* expression by qPCR, zebrafish eyes were dissected, the lens was removed, and the resultant eye cup was stored in Trizol at -80° C. RNA was extracted via Trizol-chloroform extraction, Turbo DNase (Invitrogen) treatment, and RNA cleanup using the RNeasy Mini Kit (Qiagen). cDNA was then generated by reverse transcription of 200 ng of RNA using Superscript IV reverse transcriptase (Invitrogen). The sample was then treated with RNase H (New England Biolabs) to remove RNA, and cDNA isolated using an RNeasy mini kit (Qiagen). For analysis of *thraa, thrab, thrb, lws1,* and *lws2* expression, retina and RPE were separately isolated and RNA extracted. cDNA was generated by reverse transcription of 1 µg of retina-derived and 100 ng of RPE-derived RNA.

The amplification efficiency of primer pairs was tested by creating five-point standard curves using a 1:10 dilution series of cDNA extracted from the eyes of both zebrafish treated with vehicle and TH. Primer efficiencies ranged from 97-104%. Melt curve analysis confirmed amplification of a single product. cDNA extracted from whole eyes was diluted 1:40 in water and 4 µl sample/well were run in three technical replicates. Cycling threshold (Ct) values were normalized to the Ct values of *rpl13a* or *actb2* to yield dCt values for statistical testing. Primers: *rpl13a*: 5'-TCCCAGCTGCTCTCAAGATT-3' and 5'-ACTTCCAGCCAACTTCATGG-3', *actb2*: 5'-TGACAGGATGCAGAAGGAGA-3' and 5'-GCCTCCGATCCAGACAGAGT-3', *cyp27c1*: 5'-CATGATGATCTGATCGTTGGA-3' and 5'-CGGGGGAAGTTCTCCTCAT-3', *thraa:* 5'-CAACCTGCCAGAAGGAGATG-3' and 5'-GTCGGATGTGCTGTTCATAGAG-3', *thrab:* 5'-CCCAAATCAATCAGAGGGAGAA-3' and 5'-GGGATGTACCCTTGTGAGATTG-3', *thrb*: 5'-TCCTCTGATCGTCCAGGTTTA-3' and 5'-CACCTTGTGCTTACGGTAGTT-3', *thrb2:* 5'-GATGCAAGGGCCACATAAGA-3' and 5'-GCTTTGTCTCCACAAACAACAC-3', *lws1: 5'-*TACCTGGCCATCCATGCTG-3' and 5'-GGCGAAGAACGTGTAAGGAC-3'*, lws2: 5'-* CAAGAGCGCCACCATCTAC-3' and 5'- GAGCCATCATCCACCTTCTTT-3'*.*

Immunohistochemistry. For the analysis of 5 dpf larvae, *thrb*$^{stl627/+}$ mutants were intercrossed to produce mixed genotype offspring. For the analysis of 3 dpf larvae, the following crosses were performed to produce mixed genotype offspring: *Tg(trβ2:tdTomato)*;*thrb*$^{stl627/+}$ x *thrb*$^{stl627/+}$*, Tg(trβ2:tdTomato)*;*Tg(sws1:GFP); thrb*$^{stl627/+}$ intercross, and *Tg(trβ2:tdTomato)*;*Tg(ptf1a:GFP); thrb*$^{stl627/+}$ intercross. Larvae were treated with 200 µM N-phenylthiourea (PTU; P7629, Sigma) from 24 hpf onwards to inhibit melanin synthesis. Larvae were dissected, and the retina-containing anterior segment fixed in 4% PFA with 5% sucrose overnight at 4° C. Corresponding posterior segments were genotyped to identify clutch-matched WT and *thrb*$^{-/-}$ anterior segments. After fixation, samples were treated with Proteinase K in PBS (20 µg/ml, RPROTK-RO, Sigma) for 15 min at room temperature. Larvae were then incubated in either 10% normal goat serum (NGS; 005-000-121, Jackson ImmunoResearch), or normal donkey serum (NDS; 017-000-121, Jackson ImmunoResearch) in PBS containing 1% tween-20, 1% tritonX-100, and 1% DMSO (PBS-TTD) for 1 hour at room temperature, followed by primary antibody overnight at room temperature, then secondary antibodies overnight at room temperature. Retina from 5 dpf larvae were dissected and mounted on 1% agarose in PBS with lens down and coverslipped with Vectashield (Vector Laboratories). Whole 3 dpf larvae were mounted ventral side down (with yolk sacs removed) onto glass slides, using glass coverslip fragments as risers and mounted in Vectashield.

For adult flatmount preparations, sibling WT and *thrb*$^{stl627/stl627}$ adult zebrafish retinas were isolated from dark-adapted zebrafish and the dorsal retina marked with an incision. Retinas were fixed in ~50 µl of 2% w/v trichloroacetic acid and flattened by placing a 1.5 g weight on top of a

piece of parafilm on the retina for 30 min, based on the protocol in (6). Retina were then washed in PBS and incubated in 2% NGS in PBS-TTD for 1 hr at room temperature, incubated in primary antibodies overnight at room temperature, then in secondary antibodies overnight at room temperature. 300 µl DAPI **(**4′,6-diamidino-2-phenylindole) in PBS (1µg/ml) were then added for 20 minutes at room temperature to counterstain nuclei. Alternatively, DRAQ5 (1:1000; AB108410, Abcam) was used as a nuclear counterstain. Retinas were then placed on slides coated with 1% agarose in PBS, photoreceptor side down, and mounted in Vectashield. For adult retinal sections with Arr3a and green cone opsin staining, adult vehicle-treated (see TH treatment methods) WT and *thrb*$^{stl628/stl628}$ retinas were dissected and placed in a 9:1 mixture of 100% Ethanol: 37% formaldehyde overnight at 4º C as performed in (7), then transferred to 30% sucrose overnight at 4º C. Eyes were then embedded in Optimal Cutting Temperature (OCT) compound (Tissue-Tek) and frozen on dry ice. 12 µm sections were then taken on a cryostat near the optic nerve head. Retinas were then incubated in primary antibody overnight at 4º C followed by secondary antibody for 1 hour at room temperature, and then by DAPI incubation (1µg/ml) in PBS for 30 seconds. Slides were then mounted in Vectashield and images of peripheral retina taken using a 40x oil-immersion objective on a Zeiss LSM700 confocal microscope.

For the analyses of 12 dpf CMZ, *Tg(trβ2:tdTomato)*; *Tg(sws1:GFP); thrb*$^{stl627/+}$ zebrafish were intercrossed and clutch-matched 12 dpf mixed genotype offspring were analyzed. Zebrafish were dissected, and the retina-containing anterior segment fixed in 4% PFA overnight at 4º C. Corresponding posterior segments were genotyped to identify clutch-matched WT and *thrb*$^{-/-}$ anterior segments. Anterior segments were then embedded and sectioned as described for adult zebrafish retina. To enhance the tdTomato signal, sections were then incubated in primary anti-dsRed antibody (1:200; 632496, TakaraBio) overnight at 4º C followed by secondary anti-rabbit conjugated with Alexa-555 antibody (1:1000; A31572, Invitrogen) for 1 hour at room temperature. Slides were mounted and imaged as described for adult retina.

Image Quantification. For 3 dpf larvae, optical slices of WT and *thrb*$^{stl627/stl627}$ retina were acquired using a Zeiss LSM700 confocal microscope. The number of UV-cone opsin^{+} and tdTomato^{+} cells across 76 µm were then quantified using ImageJ software. For 5 dpf larvae, the number of Arr3a^{+} cells per 1600 µm^2 were quantified in WT and *thrb*$^{stl627/stl627}$ retinas in an area immediately dorsal to the optic nerve head. For adult retina flatmount preparations, we obtained three 6900 µm^2 images from the periphery of the dorsotemporal quadrant of each retina. The number of Arr3a^{+} and Arr3b^{+} cells per image were then quantified and averaged per retina (WT or *thrb*$^{stl627/stl627}$).

High Performance Liquid Chromatography (HPLC). We used HPLC to measure the retinaldehyde content of vehicle and TH-treated zebrafish. Eyes were harvested under dim light, frozen on dry ice, and stored at -80º C. Two eyes per fish were thawed under orange light and homogenized in cold 0.9% saline with a glass dounce homogenizer. Retinaldehydes were derivatized with hydroxylamine (Sigma, 255580) and extracted in hexane. Extracts were dried under a continuous flow of nitrogen and then resuspended in 120 µl of hexane (Acros Organics, 610070040). 100 µl was injected into an Agilent 1100 series HPLC fitted with a Zorbax RX-SIL column (4.6×250 mm, 5 µm, Agilent). The samples were eluted with a gradient mobile phase consisting of 0.5% ethyl acetate in hexane for 5 min then a ramp up to 10% ethyl acetate in hexane from 5 to 20 min, followed by isocratic conditions from 20 to 30 min, then 0.5% ethyl acetate in hexane from 31 to 40 min. The column was held at 25° C, and the flow rate was 1.4 ml min^{-1}. Samples were monitored using a photodiode array detector at 325, 350 and 380 nm. Retinoid identity was determined by comparison to all-*trans*-retinaldehyde oxime standards (derivatized from *all-trans*-retinaldehyde using hydroxylamine) and published accounts (8–10). The pmol of A_1 and A_2 retinaldehyde oximes were calculated based on standard curves generated using oxime-derivatized all-*trans*-retinaldehyde. To quantify the relative proportion of A_2 retinaldehyde oximes in our samples, pmol of A_2 retinaldehyde oximes were summed and divided by the total pmol of A_1 and A_2 retinaldehyde oximes. In a small subset of samples, we detected a non-retinoid species of unknown identity that partially overlapped the A_2 form of *syn-all-trans* retinaldehyde.

RNA-seq. To perform RNA-seq on WT and *thrb*$^{stl628/stl628}$ retina, we first isolated the retinas of 6 mo WT and clutch-matched *thrb*$^{stl628/stl628}$ zebrafish. Two retinas from a male and two retinas from a female zebrafish were combined to make one sample. Three WT and *thrb*$^{stl628/stl628}$ samples were collected and RNA extracted using trizol-chloroform extraction. RNA concentrations ranged between 27-55 ng/µl, and all RNA integrity number scores were > 8.7. 2-4 µg mRNA were submitted to the Genome Technology Access Center at Washington University, where library preparation was performed as follows: First, Ribosomal RNA was removed by poly-A^+ selection using Oligo-dT beads (mRNA Direct kit, Life Technologies). Then, mRNA was fragmented in buffer containing 40 mM tris acetate pH 8.2, 100 mM potassium acetate, and 30 mM magnesium acetate heated to 94^o C for 150 seconds. Subsequently, mRNA was reverse transcribed to yield cDNA using SuperScript III RT enzyme (Life Technologies), and a second-strand reaction was performed to produce cDNA. cDNA ends were made blunt, an "A" base was added to the 3' ends, and Illumina sequencing adapters were ligated to the ends. Ligated fragments were then amplified for 12 cycles using primers incorporating unique index tags. These fragments were then sequenced on an Illumina HiSeq2500 (single-end 50bp reads). RNA-seq sequencing adapters were first trimmed using Cutadapt 1.9.1 (11). RNA-seq reads were then aligned to danRer10 using STAR 2.7.2b with an index prepared for 50 bp reads (12). HTseq 0.9.1 was then used to generate normalized read counts (13). To calculate differential gene expression and create MA plots, DESeq2 1.18.1 was used (R 3.4.3) (14).

Statistical Analysis. Changes in *cyp27c1* expression in response to TH treatment (quantified by qPCR) were evaluated by collapsing combinations of treatment status (TH vs. vehicle) and genotype (WT vs. mutant) into a single variable and performing a one-way ANOVA (F-test) followed by a Tukey's Honest Statistical Difference (HSD) test to identify significant pairwise differences while adjusting for multiple comparisons. Similarly, differences in A_2 retinaldehyde levels (quantified as the proportion of A_2 retinaldehyde to total A_1 and A_2 retinaldehydes by HPLC) were evaluated by first transforming the data as described previously followed by fitting transformed values with a beta regression model and performing a likelihood ratio test to assess the significance of the combined genotype-treatment variable (15). Post-hoc tests were again performed using Tukey's HSD test to identify significant pairwise differences in the proportion of A_2 retinaldehyde while adjusting for multiple comparisons. Student's t-tests and Mann-Whitney U tests were performed where mentioned in the legends. Statistical analyses were performed in R (v3.6.2) using the packages emmeans (v1.4.4) betareg (3.1.3), and lmtest (v0.9.37) (16-19).

Electrophysiology. 10 mo *thrb*$^{stl627/stl627}$ and age-matched WT zebrafish of both sexes were used for the *ex vivo* transretinal ERG recordings. The animals were dark-adapted overnight prior to the recordings. The fish were euthanized by initial anaesthetization in ice cold water, followed by decapitation. Eyes were enucleated under an infrared dissection microscope. After dissection and removal of the RPE, the retinas were mounted in a closed chamber (20), with the photoreceptors facing up, and were superfused with Ringer's solution containing (in mM): 111 NaCl, 2.5 KCl, 1.6 $MgCl_2$, 1 $CaCl_2$, 0.01 EDTA, 3 HEPES and 10 glucose (pH adjusted to 7.8 with NaOH) at a flow rate of 3-5 ml per minute as previously described (5). For spectral sensitivity measurements, retinas were adapted to the background illumination at 460 nm for at least 15 minutes before the experiments. *Ex vivo* transretinal ERG recordings were made by presenting light flashes produced by a tungsten 100W bulb. Flash intensity and wavelength were controlled by a combination of neutral density and interference filters (21). Absolute sensitivity was calculated as the ratio of the dim-flash b-wave response amplitude (< 30% of the saturated response) and its corresponding flash intensity. Fractional sensitivity (S_f) was calculated by normalizing the absolute sensitivity to the corresponding maximal saturated b-wave response. The ERG signals were amplified using a differential amplifier (Warner Instruments), low-pass filtered at 300Hz (Krohn Hite Corp.), digitized using Digidata 1322A (Axon Instruments), and recorded at a sampling frequency of 10kHz using pClamp 10 software. Data were analyzed offline using Clampfit 10, Microsoft Excel and Origin 2018 and presented as mean ± SEM. Student's t-tests were used for significance testing.

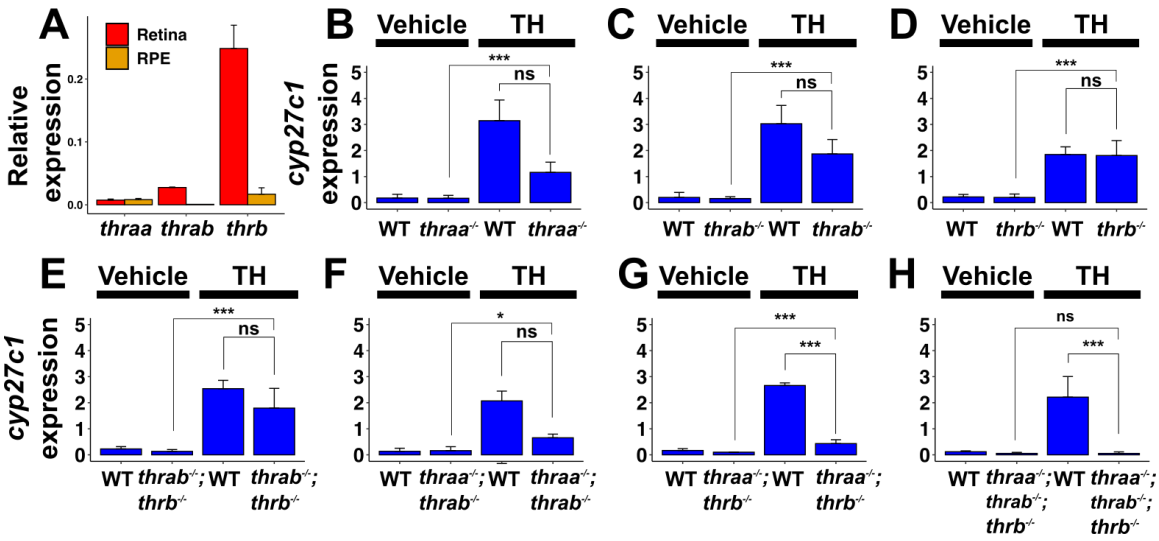

Figure S1. qPCR experiments repeated using *actb2* as a reference gene (A) Quantification of TH receptor expression in the retina and RPE of 5 mo WT zebrafish by qPCR. Relative expression (normalized to *actb2* expression [2^{-dCt}]; mean ± SD; n = 3 for all transcripts, except n = 1 for *thrab* in RPE due to lack of detectable transcript in two samples). (B-H) Adult (> 2 mo) WT and TH receptor mutants were treated with either vehicle or TH (300 µg/l L-thyroxine) for three weeks and then harvested for analysis by qPCR (*cyp27c1* expression). (B-D) TH-induced expression of *cyp27c1* (normalized to *actb2* expression [2^{-dCt}]; mean ± SD) is maintained in all three TH receptor mutants, (E-H) Induction of *cyp27c1* expression is attenuated in *thraa*$^{-/-}$;*thrb*$^{-/-}$ double mutants and completely lost in *thraa*$^{-/-}$;*thrab*$^{-/-}$;*thrb*$^{-/-}$ fish. (n = 4 per experimental group in B-H). Experiments shown in panels B-H were evaluated by one-way ANOVA (F-test) followed by a Tukey's Honest Significant Difference test to assess pairwise differences while adjusting for multiple comparisons. *thrb*$^{-/-}$ = *thrb*$^{stl627/stl627}$ in all experiments. ***adjusted p < 0.001; **adjusted p < 0.01; *adjusted p < 0.05; ns, not significant.

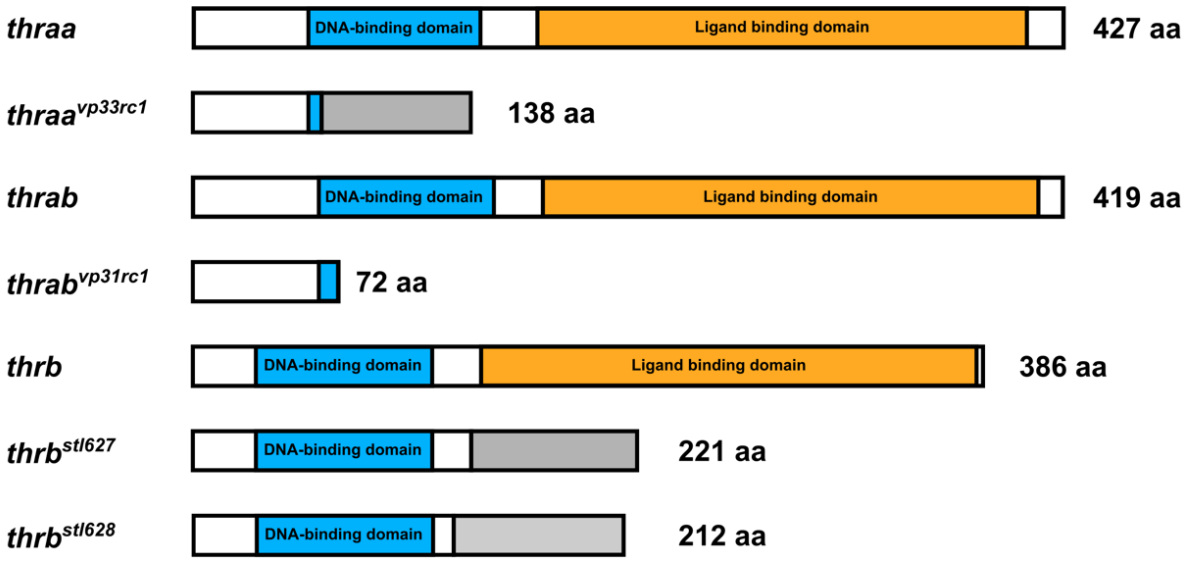

Figure S2. Diagram of all WT and mutant TH receptor protein domain architectures. Grey bars refer to protein product following frameshift mutation. No grey bar is visible in the *thrab*^{vp31rc1} as a stop codon is created at the site of mutation. aa, amino acids in protein product.

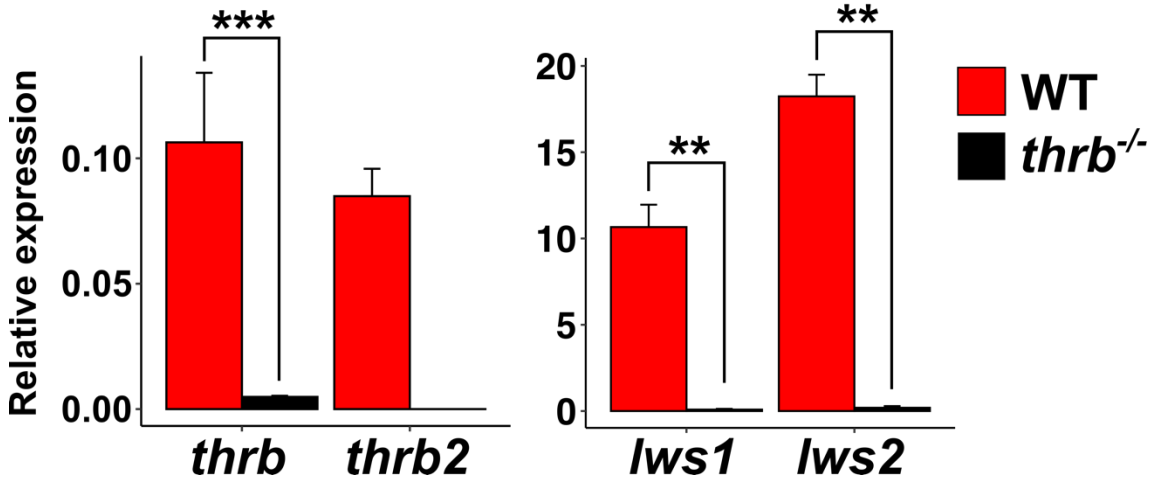

Figure S3. qPCR analysis of *thrb* (with primers that detects all isoforms), *thrb2* (with primers specific to *thrb2*), *lws1,* and *lws2* expression in vehicle-treated 5 mo *thrb*$^{-/-}$ retina. Relative expression (normalized to *rpl13a* expression [2^{-dCt}]; mean ± SD; n = 3 for all transcripts). *thrb*$^{-/-}$ = *thrb*$^{stl627/stl627}$. No *thrb2* transcripts were detected in two of three *thrb*$^{-/-}$ samples, so no statistical analyses were performed. All remaining statistical analyses were performed using two-tailed t-tests. *** p < 0.001; ** p < 0.01; *p < 0.05.

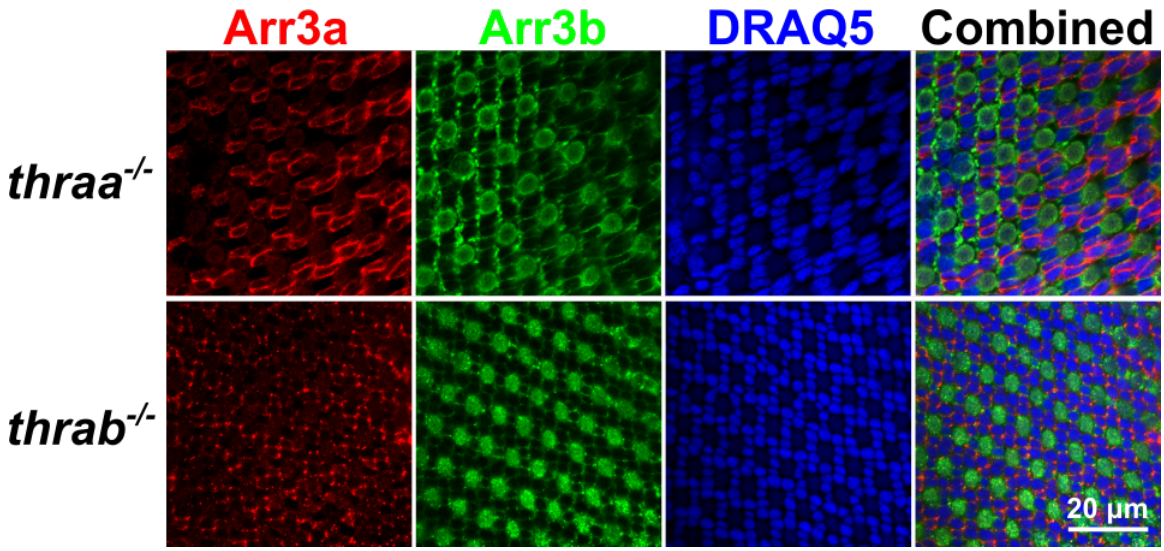

Figure S4. Flatmount images of 3 mo *thraa*$^{-/-}$ and *thrab*$^{-/-}$ retina stained with Arr3a antibody (red and green cones), anti-Arr3b antibody (blue and UV cones), and DRAQ5 (nuclei) (n = 1).

Dataset S1 (separate file). List of differentially expressed genes in 6 month-old WT and *thrb*$^{-/-}$ retina as determined by DEseq2 (14). Highlighted genes are those with FDR < 0.05, as shown in Fig. 5. *thrb*$^{-/-}$ = *thrb*$^{stl628/stl628}$. FDR; False Discovery Rate (adjusted *P* value).

SI References

1. M. A. Moreno-Mateos, *et al.*, CRISPRscan: Designing highly efficient sgRNAs for CRISPR-Cas9 targeting in vivo. *Nat. Methods* **12**, 982–988 (2015).

2. M. Haeussler, *et al.*, Evaluation of off-target and on-target scoring algorithms and integration into the guide RNA selection tool CRISPOR. *Genome Biol.* **17**, 1–12 (2016).

3. W. Y. Hwang, *et al.*, Efficient genome editing in zebrafish using a CRISPR-Cas system. *Nat. Biotechnol.* **31**, 227–229 (2013).

4. J. M. Trimarchi, *et al.*, Molecular Heterogeneity of Developing Retinal Ganglion and Amacrine Cells Revealed through Single Cell Gene Expression Profiling. *J. Comp. Neurol.* **502**, 1047–1065 (2007).

5. J. M. Enright, *et al.*, Cyp27c1 red-shifts the spectral sensitivity of photoreceptors by converting Vitamin A1 into A2. *Curr. Biol.* **25**, 3048–3057 (2015).

6. G. Salbreux, L. K. Barthel, P. A. Raymond, D. K. Lubensky, Coupling Mechanical Deformations and Planar Cell Polarity to Create Regular Patterns in the Zebrafish Retina. *PLoS Comput. Biol.* **8** (8), doi:10.1371/journal.pcbi.1002618 (2012).

7. J. L. Thomas, C. M. Nelson, X. Luo, D. R. Hyde, R. Thummel, Characterization of multiple light damage paradigms reveals regional differences in photoreceptor loss. *Exp. Eye Res.* **97**, 105–116 (2012).

8. D. Babino, B. D. Perkins, A. Kindermann, V. Oberhauser, J. Von Lintig, The role of 11-cis-retinyl esters in vertebrate cone vision. *FASEB J.* **29**, 216–226 (2015).

9. M. A. Kane, J. L. Napoli, Quantification of Endogenous Retinoids. *Methods in Molecular Biology.* **652**, 1-54 (2010).

10. A. Morshedian, *et al.*, Cambrian origin of the CYP27C1-mediated vitamin A_1-to-A_2 switch, a key mechanism of vertebrate sensory plasticity. *R. Soc. Open Sci.* **4** (7), 170362 (2017).

11. M. Martin, Cutadapt removes adapter sequences from high-throughput sequencing reads. *EMBnet.journal* **7**, 10–12 (2011).

12. A. Dobin, *et al.*, STAR: Ultrafast universal RNA-seq aligner. *Bioinformatics* **29**, 15–21 (2013).

13. S. Anders, P. T. Pyl, W. Huber, HTSeq-A Python framework to work with high-throughput sequencing data. *Bioinformatics* **31**, 166–169 (2015).

14. M. I. Love, W. Huber, S. Anders, Moderated estimation of fold change and dispersion for RNA-seq data with DESeq2. *Genome Biol.* **15**, 550 (2014).

15. Smithson M, Verkuilen J. A better lemon squeezer? Maximum-likelihood regression with beta-distributed dependent variables. *Psychol Methods* **11**, 54–71 (2006).

16. R Core Team. R: A language and environment for statistical computing. R Foundation for Statistical Computing, Vienna, Austria. https://www.R-project.org/ (2018).

17. Lenth R. emmeans: Estimated Marginal Means, aka Least-Squares Means. R package, Version 1.4.4. https://CRAN.R-project.org/package=emmeans (2020).

18. Cribari-Neto F, Zeileis A. Beta Regression in R. Journal of Statistical Software **34**, 1-24

(2010).

19. Zeileis A, Hothorn T. Diagnostic Checking in Regression Relationships. R News **2**, 7-10. https://CRAN.R-project.org/doc/Rnews/ (2008).

20. F. Vinberg, V. Kefalov, Simultaneous ex vivo functional testing of two retinas by in vivo electroretinogram system. *J. Vis. Exp.*, e52855 (2015).

21. A. V. Kolesnikov, P. H. Tang, R. O. Parker, R. K. Crouch, V. J. Kefalov, The mammalian cone visual cycle promotes rapid M/L-cone pigment regeneration independently of the interphotoreceptor retinoid-binding protein. *J. Neurosci.* **31**, 7900–7909 (2011).